

Self-Powered Electrostatic Adsorption Face Mask Based on a Triboelectric Nanogenerator

Guoxu Liu,^{†,‡,§} Jinhui Nie,^{†,‡,§} Changbao Han,^{†,‡,§} Tao Jiang,^{†,‡,§} Zhiwei Yang,^{†,‡,§} Yaokun Pang,^{†,‡,§} Liang Xu,^{†,‡,§} Tong Guo,^{†,‡,§} Tianzhao Bu,^{†,‡,§} Chi Zhang,^{*,†,‡,§,||} and Zhong Lin Wang^{*,†,‡,§,||}

[†]Beijing Institute of Nanoenergy and Nanosystems, Chinese Academy of Sciences, Beijing 100083, China

[‡]CAS Center for Excellence in Nanoscience, National Center for Nanoscience and Technology (NCNST), Beijing 100190, China

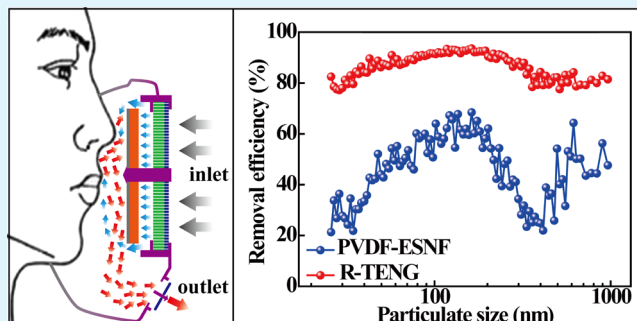
[§]University of Chinese Academy of Sciences, Beijing 100049, China

^{||}School of Material Science and Engineering, Georgia Institute of Technology, Atlanta, Georgia 30332, United States

Supporting Information

ABSTRACT: The physical filtration mechanism of a traditional face mask has a low removal efficiency of ultrafine particulates in the size range of 10–1000 nm, which are badly harmful to human health. Herein, a novel self-powered electrostatic adsorption face mask (SEA-FM) based on the poly(vinylidene fluoride) electrospun nanofiber film (PVDF-ESNF) and a triboelectric nanogenerator (TENG) driven by respiration (R-TENG) is developed. The ultrafine particulates are electrostatically adsorbed by the PVDF-ESNF, and the R-TENG can continually provide electrostatic charges in this adsorption process by respiration. On the basis of the R-TENG, the SEA-FM shows that the removal efficiency of coarse and fine particulates is higher than 99.2 wt % and the removal efficiency of ultrafine particulates is still as high as 86.9 wt % after continually wearing for 240 min and a 30-day interval. This work has proposed as a new method of wearable air filtration and may have great prospects in human health, self-powered electronics, and wearable devices.

KEYWORDS: electrostatic adsorption, face mask, triboelectric nanogenerator, self-powered, PVDF nanofiber



INTRODUCTION

With the rapid industrialization, urbanization, and increasing energy consumption in developing countries, particulate pollution has attracted more and more attention because of its severe impact on public health.^{1–4} Although the ultrafine particulates are only tiny components of the atmospheric composition, they exert a significant influence on air quality and visibility.^{5–7} Compared with coarse particulates (the diameter within 2.5–10 μm) and fine ones (the diameter within 1.0–2.5 μm), the ultrafine particulates (the diameter less than 1.0 μm) are characterized by carrying a large amount of poisonous and harmful substances, which can remain in the atmosphere for a long time and spread far away.⁸ Studies have demonstrated that the smaller particulates are more likely to penetrate deeper site of the respiratory tract of human being and deposit in bronchioles and alveoli, which will affect the ventilator function of lungs and make the body easy hypoxia.^{9–11} Nowadays, wearable air purification devices with the traditional physical filtration mechanism (PFM), including diffusion, inertial impaction, interception, and gravity, can prevent injury from coarse particulates, but either have a very limited filtration effect for fine particulates, especially ultrafine ones, or at the expense of breathability.^{12–15} Moreover, activated carbon adsorption is applied to many wearable air purification devices to improve

the filtration efficiency, but its short life cycle limits its wide application.¹⁶ An effective and long-term filtration mechanism for ultrafine particulates plays an essential role in public health protection, which is expected for wide applications in wearable air purification devices.

Over past few years, the triboelectric nanogenerator (TENG) is fabricated to harvest a great variety of mechanical energy such as wind,¹⁷ water wave,^{18,19} and vibration.²⁰ Recently, the TENG has been used for harvesting energy from human motion, such as walking, running, and clapping.^{21–23} Previous work on TENGs has demonstrated the fundamental theory lies in the second term of Maxwell's displacement current. On the basis of contact electrification and electrostatic induction, the open-circuit voltage generated by the TENG is hundreds of times higher than that generated by electromagnetic generators.^{24–26} For example, a planar sliding TENG as active microactuators for optical modulation invented by Zhang et al. can generate a dual-channel open-circuit voltage as high as 2 kV when the sliding displacement is 70 mm.^{27,28} A TENG fabricated by Han et al. can generate a space electric field as high as 12 MV/m,

Received: December 9, 2017

Accepted: February 2, 2018

Published: February 2, 2018

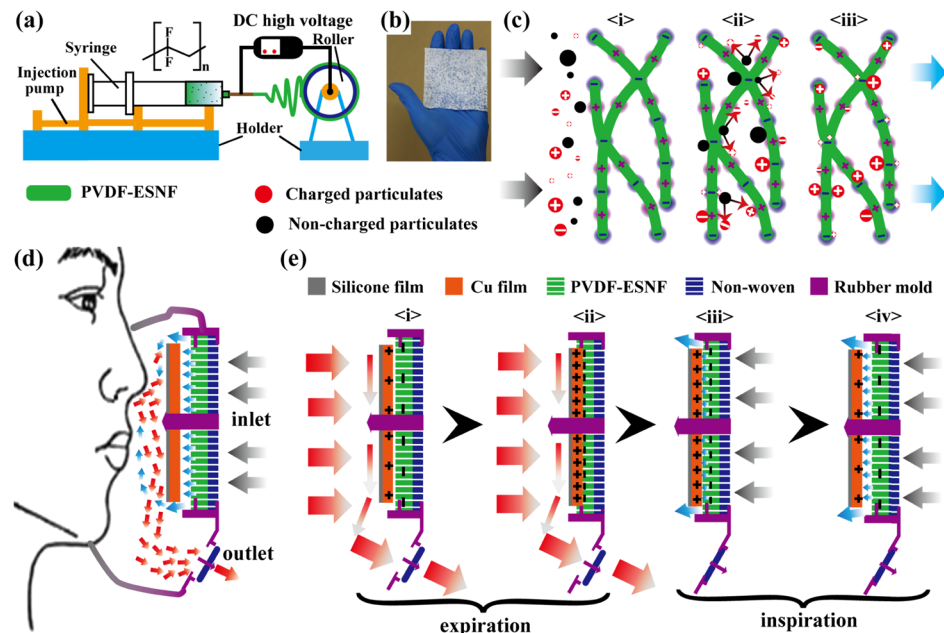


Figure 1. Fabrication, structure, and working principles of the TENG driven by respiratory (R-TENG) based on the PVDF-ESNF. (a) Schematics of fabricating PVDF-ESNF by electrospun. The inset is the general molecular structure of PVDF. (b) Photo of the PVDF-ESNF. (c) Schematic filtration mechanism of the PVDF-ESNF. (i) Charged and noncharged particulates flow through the PVDF-ESNF with the airflow. (ii) By the contact electrification and the charge polarization, the noncharged particulates are charged by the PVDF-ESNF and the charged ones are absorbed by the PVDF-ESNF. (iii) By coupling PFM and electrostatic adsorption, the particulates in the airflow are filtered out. (d) Structure of the R-TENG for the self-powered electrostatic absorption face mask (SEA-FM). (e) Working principles of the R-TENG by periodic expiration and inspiration. (i) Cu film is pushed to PVDF-ESNF, (ii) Cu film and PVDF-ESNF are in contact on the expiration state. (iii) Cu film is separated from the PVDF-ESNF, and (iv) gap between the Cu film and the PVDF-ESNF increases to the maximum on the inspiration state.

and a self-power filter applies for automobile exhaust based on this TENG which has a removal efficiency of about 95.5% for PM_{2.5}.²⁹ Gu et al. invent a polyimide nanofiber filter enhanced by the rotating TENG which has the highest enhancement efficiency of 207.8% at a diameter of 76.4 nm.³⁰ Nowadays, wearable self-powered devices by harvesting biomechanical energy are receiving intensive research endeavor.³¹ Breathing as a biomechanical energy is a low-frequency periodic motion, which is very promising to be harvested by the TENG for wearable self-powered air purification device.

Here in this work, a self-powered electrostatic adsorption face mask (SEA-FM) with a low pressure drop based on the R-TENG and electrospun is fabricated. Utilizing the R-TENG based on the poly(vinylidene fluoride) electrospun nanofiber film (PVDF-ESNF), the SEA-FM can effectively remove particulates especially the ultrafine ones, in which the R-TENG continually provides electrostatic charges for the PVDF-ESNF. During a 240 min wearing experiment with a 30-day interval, the removal efficiency of coarse and fine particulates is higher than 99.2 wt % due to coupling electrostatic adsorption and PFM, whereas the removal efficiency of ultrafine particulates maintains at more than 86.9 wt %, in which the average pressure drop is 170 Pa with the wind speed of 30 cm/s. The high removal efficiency, low pressure drop, and long-term service life are validated for protecting human health from air pollution. This work exhibits a new air purification mode of self-powered wearable devices and might provide a potential application in human health, self-powered electronics, and wearable devices.

■ RESULTS AND DISCUSSION

Filtration Mechanism of the PVDF-ESNF and Working

Principles of the R-TENG. The fabrication, structure, and working principles of the R-TENG are schematically illustrated in Figure 1. The PVDF-ESNF is prepared on a nonwoven substrate by electrospun from diverse polymer solutions with controllable dimensions, as illustrated in Figure 1a. The inset of Figure 1a shows a general molecular structure of PVDF, and Figure 1b is the photo of the PVDF-ESNF. Figure 1c shows the filtration mechanism of the PVDF-ESNF by coupling the PFM and electrostatic adsorption. When the air mixed with the particulates flows through the PVDF-ESNF (Figure 1c(i)), the coarse particulates are filtered out by the PFM. For the fine and especially ultrafine ones, the charged ones (red ball) are absorbed by the negative or positive area on the PVDF-ESNF, which is saturated with electrostatic charges (the overall showed negative potential) after the process of electrospun, as shown in Figure 1c(ii). While, the uncharged ones (black ball) contact with and are charged by the PVDF-ESNF for the mechanism of contact electrification and charges polarization. Then, all of the charged particulates are absorbed and immersed deep into the membrane, as shown in Figure 1c(iii).

The R-TENG is implanted into the inlet of a face mask where the airflow of the breath is most concentrated, as schematically illustrated in Figure 1d. The basic structure of the R-TENG in the contact-separation mode is composed of a Cu film, a silicon film, a nonwoven, a rubber mold, and a PVDF-ESNF, which serves as triboelectric and filtration layers. The structure of the testing apparatus for the R-TENG is shown in Figure S1, and the detailed fabrication processes can be found in the [Assembly and Characterization of the R-TENG and SEA-FM](#). As is known to all, vapor affects the production of

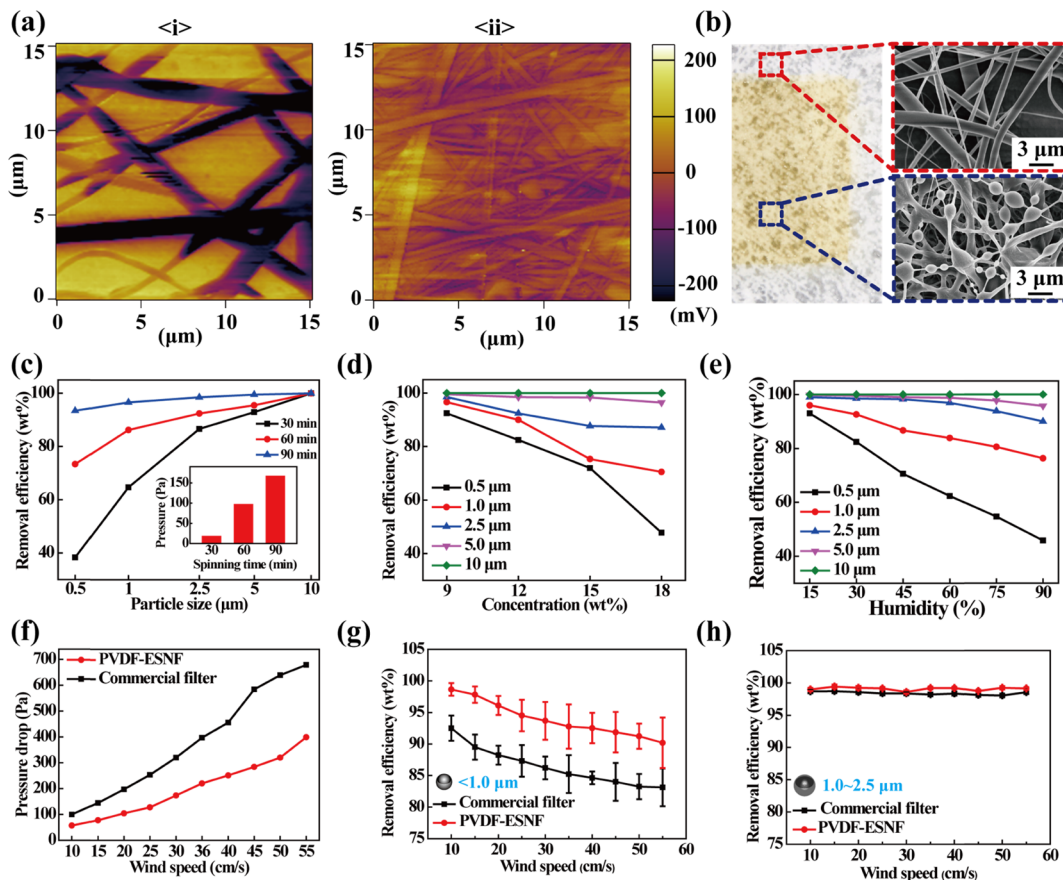


Figure 2. Particulate matters removal characteristics of the PVDF-ESNF. (a) (i,ii) Microscopic potential (i) before and (ii) after adsorption. (b) Macroscopic and microscopic changes of the filter membrane before (enlarged view with red dashed line) and after adsorption (enlarged view with blue dashed line). (c) Removal efficiency vs particulate size at different electrospun times. The inset is the corresponding pressure drop of the PVDF-ESNF at different electrospun times when the airflow is 30 cm/s. (d) Removal efficiency vs concentration of the PVDF solution at different particulate sizes. (e) Removal efficiency vs humidity of filtration process at different particulate sizes. (f) Pressure drop of the PVDF-ESNF and the filter membrane in commercial mask vs wind speed. The removal efficiency of the PVDF-ESNF and the filter membrane in the commercial mask vs wind speed at particulate sizes (g) less than 1.0 μm and (h) from 1.0 to 2.5 μm .

electrostatic charges and the removal efficiency of electrostatic adsorption. To ensure the expired gas with heat and vapor flows out immediately from the face mask, the inhaling and exhaling parts of the mask are separated. With such a configuration, the vapor will not flow into the R-TENG, which can maintain the amount of electrostatic charges and extend the service life of the PVDF-ESNF. The R-TENG can continually provide electrostatic charges for the PVDF-ESNF in the duration of electrostatic adsorption (Figure 1e). On the expiratory state, when the gas expels from the nose or mouth, a positive pressure is applied to the silicon film which is attached to the Cu film and the airflow will push the Cu film close to the PVDF-ESNF (Figure 1e(i)). Then, the inlet is closed and the outlet is opened due to the high pressure drop. The airflow will be forced out from the outlet of the face mask immediately, which is schematically shown in Figure 1e(ii). For the reason that PVDF is much more triboelectrically negative than Cu, electrons are injected from the Cu film into the PVDF-ESNF, leaving net positive charges on the Cu film and net negative charges on the PVDF-ESNF for triboelectrification. The produced triboelectric charges with opposite polarities are fully balanced at this moment. Although on the inspiratory state, lung capacity leads to a higher pressure drop in the chamber of the face mask; the mobile Cu film is separated from the fixed PVDF-ESNF for a certain distance (Figure 1e(iii)).

The airflow draws through the PVDF-ESNF first and then sweeps past the surface of the Cu film. The particulates are filtered out by the coupling mechanism of PFM and electrostatic adsorption. Until the inhalation process over, the two layers of the R-TENG reach the maximum separation distance and the charge density of the PVDF-ESNF decreases to the minimum for the charge neutralization in the course of the electrostatic adsorption, as shown in Figure 1e(iv). Once the human exhales again, lung capacity will immediately form positive air pressure in the chamber so that two triboelectric layers (Cu film and PVDF-ESNF) will contact each other again. The dynamic process of breathing exerts the periodic force upon the R-TENG, which will generate steady triboelectric charges on the surface of the PVDF-ESNF and Cu film.

To predict the generated electric field by the R-TENG, the potential distribution of the R-TENG in the respiration process is calculated by a finite element method (FEM) in the COMSOL software, as shown in Figure S2. In the FEM model, the potential between the Cu film and the PVDF-ESNF is investigated. At the contacting state, the simulated electrical potential difference between the two layers is zero, as shown in Figure S2(i). When the Cu film with positive surface charges separates with the PVDF-ESNF gradually, the potential difference between the two layers increases gradually, as shown in Figure S2(ii). Finally, when the distance between

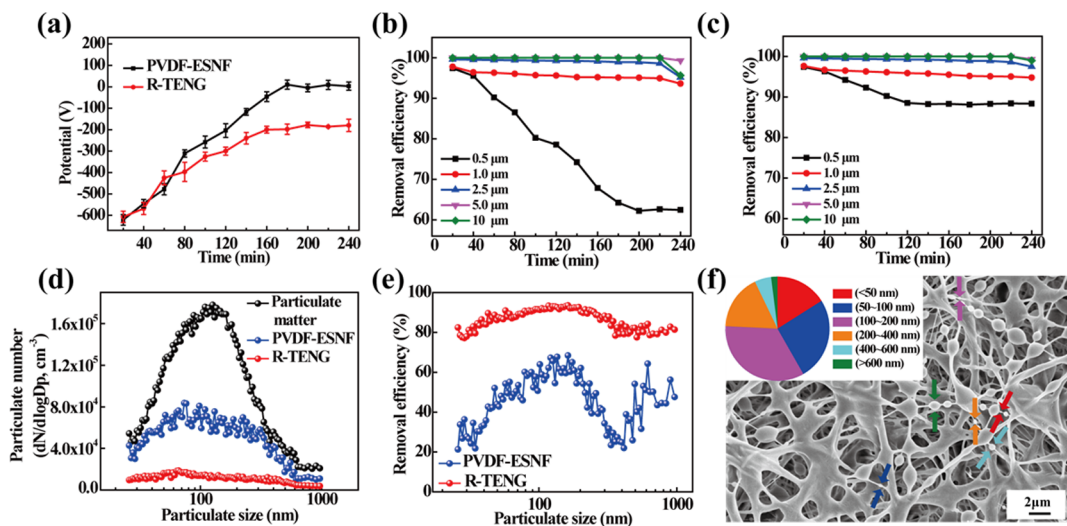


Figure 3. Characteristics comparison of the PVDF-ESNF and the R-TENG. (a) Average surface potential change of the single PVDF-ESNF and the PVDF-ESNF implanted in the R-TENG in 240 min filtration. Durability test on the removal efficiency of (b) PVDF-ESNF and (c) R-TENG. (d) Number distributions of the filtered ultrafine particulates in the size range of 25 nm to 1 μm by the PVDF-ESNF and R-TENG. (e) Corresponding removal efficiency of the PVDF-ESNF and R-TENG. (f) SEM image of the PVDF-ESNF after particulates filtration. Inset: size distribution of the absorbed particulates.

them reaches the maximum, the potential difference increases to 2046 V, as shown in Figure S2(iii). For the respiration cycles, the simulation results indicate that the periodic electric field as high as ~ 2 kV can be generated by the R-TENG for particulates adsorption.

Characterization of the PVDF-ESNF. During the adsorption process, the surface potential of each nanofiber changes a lot, as shown in Figure 2a. After 4 h, the surface potential of PVDF nanofibers changes from the initial state with a minimum of about -230 mV (Figure 2a(i)) to nearly 0 mV (Figure 2a(ii)) relative to a Cu substrate as the reference electrode. The corresponding microscopic morphology is shown in Figure S3(i,ii). In the initial state, the surface of PVDF nanofibers is saturated with electrostatic charges. While after filtration, the charges tend to disappear, which means electrostatic adsorption is involved in the filtration mechanism of the PVDF-ESNF. Meanwhile, the surface potential variations of single PVDF-ESNF and the PVDF-ESNF implanted in the R-TENG are shown in Figure S4. The color of the PVDF-ESNF changes from white to yellow after adsorption, as shown in Figure 2b. The scanning electron microscopy (SEM) images of the nonadsorption area (enlarged view with red dashed line) and adsorption area (enlarged view with blue dashed line) are shown in the insets of Figure 2b. Compared with the nonadsorption area, the adsorption area contains various particulate matters. The above results demonstrate the adsorption ability of the PVDF-ESNF.

To obtain the optimal parameters of the PVDF-ESNF when simultaneously taking the pressure drop and removal efficiency into consideration, three PVDF-ESNFs with different electrospun times (30, 60, and 90 min) are chosen. The removal efficiency in the diameter range from 0.5 to 10 μm is illustrated in Figure 2c, and the inset is the corresponding pressure drops of the PVDF-ESNFs with a wind speed of 30 cm/s in different electrospun times. The experimental results denote that the removal efficiency is increased with the increasing electrospun time. For the particulates size from 0.5 to 1.0 μm , the removal efficiency is increased from 34 to 93 wt %. This phenomenon can be ascribed to such a reason that the PVDF-ESNF has

better compactness with longer electrospun time. The PVDF-ESNF with the appropriate density and pressure drop will increase the probability of collisions between particulates and nanofibers, in which the ultrafine particulates can be captured by electrostatic force more easily. Figure 2d shows the removal efficiency versus concentration of the PVDF solution in different particulate sizes. The experimental results indicate that the removal efficiency is decreased with the increasing concentration of solution. The SEM images of the PVDF-ESNFs before and after filtration are shown in Figure S5. It is worth noting that with the increasing solution concentration and viscosity, the diameter of the nanofiber increases significantly. Different concentrations have little effects on the removal efficiency for the coarse particulates (>2.5 μm). However, for fine particulates, especially ultrafine particulates (<1.0 μm), the removal efficiency is decreased from 93 to 43 wt % with the concentrations increasing, which can be ascribed to the predominance of the electrostatic adsorption effect over the PFM, and the charges are more likely to concentrate on small-scale nanofibers. The water vapor accompanied with human respiration has significant influence on the filtration performance of the PVDF-ESNF. Figure 2e shows that the removal efficiency is decreased with the increasing humidity of filtration environment. Especially for the particulates in sizes of 0.5 μm and below, the removal efficiency is decreased from 93 to 41 wt %.

Figure 2f shows the pressure drop of the PVDF-ESNF and the filter membrane in the commercial mask versus wind speed from 10 to 55 cm/s which is in simulation with the human respiration rate. The experimental results show that the pressure drop is increased from 100 to 700 Pa with the increasing wind speed for the filter membrane in the commercial mask, whereas from 57 to 402 Pa for the PVDF-ESNF. The corresponding removal efficiencies are schematically shown in Figure 2g (<1.0 μm) and 2h (1.0–2.5 μm). Although both have almost same removal efficiencies for the fine particulates, the removal efficiency of the PVDF-ESNF is much higher than that of the filter membrane in the commercial mask for the ultrafine particulates. For the

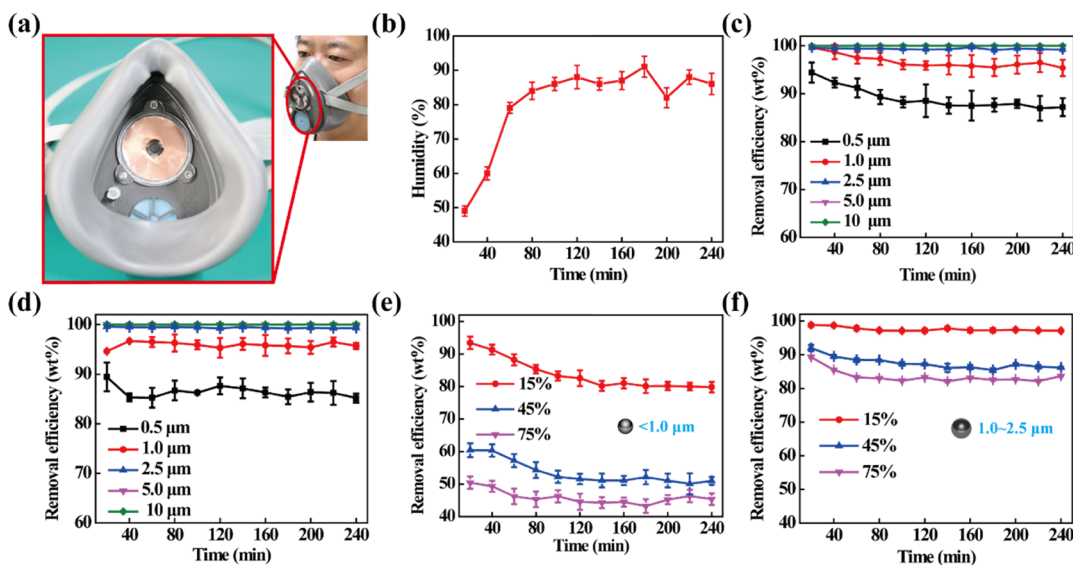


Figure 4. Characteristics of the SEA-FM based on the R-TENG. (a) Photo of the SEA-FM. (b) Internal humidity variation of the SEA-FM in the wearing process of 240 min. (c) Durability test on the removal efficiency of the SEA-FM. (d) Durability test on the removal efficiency of the SEA-FM after 30 days. Durability test on the removal efficiency of the SEA-FM in different external humidities at particulate sizes (e) less than $1.0\text{ }\mu\text{m}$ and (f) from 1.0 to $2.5\text{ }\mu\text{m}$.

particulates size from 0.5 to $1.0\text{ }\mu\text{m}$, the removal efficiency of the PVDF-ESNF is decreased from 99.4 to 90.5 wt\% , whereas that of the filter membrane in the commercial mask is decreased from 93.3 to 83.6 wt\% because of the denser and more uniform characteristics of the PVDF-ESNF. These results indicate that the PVDF-ESNF has not only the same removal effects with the filter membrane in the commercial mask for coarse and fine particulates but also a higher efficiency removal effects for ultrafine particulates.

Characterization of PVDF-ESNF and R-TENG. In the filtration process, the average surface potential change is monitored and recorded in real time, as shown in Figure 3a. It is clear to see that the average surface potential of single PVDF-ESNF changes from -600 to 0 V . Although implanted in the R-TENG, the potential remains stable around -190 V after 240 min adsorption. The removal efficiency versus filtration time at different diameter sizes is shown in Figure 3b (PVDF-ESNF) and 3c (R-TENG). The experimental results indicate that the removal efficiency is decreased with the increasing filtration time. For the particulates in sizes of $1.0\text{ }\mu\text{m}$ and above, the removal efficiency of the single PVDF-ESNF and R-TENG is higher than 97.5 wt\% in 240 min filtration, in which both of them remains almost same. For the particulates in sizes of $0.5\text{ }\mu\text{m}$ and below, the removal efficiency of the R-TENG is decreased only from 98 to 88.9 wt\% in 240 min, whereas that of the single PVDF-ESNF has a very rapid decrease from 97.4 to 62.4 wt\% . The result shows that the R-TENG has more electrostatic adsorption capacity than single PVDF-ESNF, which is consistent with the experiment results in Figure 3a.

With the 240 min filtration, the number distributions of the filtered ultrafine particulates by the PVDF-ESNF and R-TENG in the size range from 25 nm to $1\text{ }\mu\text{m}$ are measured by an electrical low-pressure impactor and schematically illustrated in Figure 3d. The unfiltered particulates number distribution curve initially rises and then drops, showing a maximum value of 1.8×10^5 in the size of 126.3 nm , and the filtered particulates number distribution curves by the PVDF-ESNF and R-TENG show the similar tendency. In the size of 126.3 nm , the

numbers decline to 6.1×10^4 and 1.2×10^4 , respectively. The corresponding removal efficiencies by the PVDF-ESNF and R-TENG are schematically illustrated in Figure 3e, in which the removal efficiency of the PVDF-ESNF varies from 32.3 to 68.4% , whereas that of the R-TENG reaches a stable level from 77.5 to 93.5% . The SEM image of the PVDF-ESNF after particulates filtration is illustrated in Figure 3f, and particulates in different sizes are listed in the inset. The particulate number in the size range of 100 – 200 nm is maximum, which accounts for 34% of all absorbed particulates. The particulate size in the range of 50 – 100 nm accounts for 25.6% , the size lower than 50 nm accounts for 17% , and closely followed is 16% in the range of 200 – 400 nm . By contrast, the particulate numbers in the range of 400 – 600 nm and higher than 600 nm make the smallest ones, which are 5.1 and 2% , respectively. Moreover, the number distributions and removal efficiency of the filtered coarse particulates by the PVDF-ESNF and R-TENG in the size range from 1.0 to $10\text{ }\mu\text{m}$ are shown in Figure S6, which remain almost the same for the PVDF-ESNF and R-TENG. The experimental results indicate that the R-TENG can supply electrostatic charges to the PVDF-ESNF by human respiratory, which has greatly enhanced removal efficiency and durability for ultrafine particulates and exhibited strong capability of TENG for self-powered electrostatic adsorption.

Characterization of SEA-FM in the Wearing Process. The photo of the SEA-FM is shown in Figure 4a, and the fabrication process can be found in the **Assembly and Characterization of the R-TENG and SEA-FM**. In the wearing process of 240 min, the internal humidity variation of the SEA-FM is shown in Figure 4b. The experimental results indicate that with the increasing wearing time, the internal humidity increases from 49 to 91% and then slightly declines to 86% , which can be ascribed to the accumulation effect of exhaled vapor. The removal efficiency versus wearing time at different diameter sizes is shown in Figure 4c. The experimental results show that the removal efficiency is decreased with the increasing wearing time. For the particulates in sizes of $0.5\text{ }\mu\text{m}$ and below, the removal efficiency of SEA-FM is decreased

from 94.4 to 86.9 wt % and then remains stable during the wearing process of 240 min. For the particulates in sizes of 1.0 μm and above, the removal efficiency is higher than 99.2 wt %. Then, with a 30-day interval, the SEA-FM is measured again at the same experimental condition, in which the removal efficiency of particulates in sizes of 0.5 μm and below maintains the same level and even has a slight increase (about 89.4 wt %). For the particulates in sizes of 1.0 μm and above, the removal efficiency remains almost the same, as shown in Figure 4d. For the different humidities of the external environment, the filtration effect of the SEA-FM is also measured, as shown in Figure 4e (<1.0 μm) and Figure 4f (1.0–2.5 μm). The experimental results indicate that for the particulates in sizes of 1.0 μm and below, the removal efficiency dramatically decreases with the increasing humanity of environment, whereas for the particulates in sizes of 1.0–2.5 μm , the removal efficiency slightly decreases with the increasing humanity, which is consistent with the results in Figure 2e. The experimental results illustrate that the SEA-FM have high removal efficiency and great durability in practical applications.

CONCLUSIONS

In summary, by coupling the PVDF-ESNF and an R-TENG in contact and separation modes, the SEA-FM has been proposed and the particulates removal characteristics are investigated in detail. The R-TENG can supply electrostatic charges to the PVDF-ESNF by human respiratory, which has greatly enhanced the removal efficiency and filtration life for ultrafine particulates. After working continually for about 240 min and a 30-day interval, the SEA-FM based on the R-TENG shows that the removal efficiency of coarse and fine particulates is higher than 99.2 wt %, and the removal efficiency of ultrafine particulates is still as high as 86.9 wt % with a low pressure drop, which is higher than that of the filter membrane in the commercial mask. This work has great potentials in the self-powered air purification device and will expand a potential application in human health, self-powered electronics, and wearable devices.

EXPERIMENTAL SECTION

Fabrication of the PVDF-ESNF. The fabrication procedure of the PVDF-ESNF is based on a far-field electrospun process. The PVDF powder with an average M_w of 530 000 is dissolved into the mixture of dimethyl formamide and acetone (3:7 in volume) at diverse percent of mass (9, 12, 15, and 18%), and then stirred at a temperature of 60 °C for 1 h until solutions become homogeneous and clear. Subsequently, the solutions are filled in 10 mL plastic syringes and fed at a constant speed of 2 mL/h through a micro pump. The positive node of a high voltage supply is connected to the syringe needle with a bias voltage around 10 kV. The drum with a diameter of 8 cm covering a nonwoven fabric is placed 10 cm away from the needle and connects to a negative node with a bias voltage around 2 kV. The rotation speed of 500 rpm is set for the drum to effectively collect aligned nanofibers. After continuously collecting for about 1.5 h, the nanofiber arrays form a film with a thickness of about 60 μm . Finally, the nanofiber film is annealed at a temperature of 60 °C for 5 h in a vacuum drying oven.

Assembly and Characterization of the R-TENG and SEA-FM. The structure of the testing apparatus for the R-TENG is composed of a Cu film (10 μm in depth), a flexible silicon film (100 μm in depth), the PVDF-ESNF, a nonwoven (10 g/m²), and an acrylic tune with its inner diameter of 50 mm. First, the PVDF-ESNF is cut into a circle ring with an inner diameter of 6 mm and an outer diameter of 54 mm and then fixed to inlet. The Cu film and the silicon film are stuck together tightly with a tape and then cut into a circle ring with an inner diameter of 6 mm and an outer diameter of 50 mm. Next, the Cu film

serving as the moving object is mounted onto the acrylic-based sliding column. Finally, all parts are fixed together with a flange (Figure S1, Supporting Information). By adjusting the volume and frequency of the airflow, the respiratory movement is simulated through the pneumatic test system (4610) (Figure S1b, Supporting Information). The SEM images are taken by using the SU8020 with an acceleration voltage of 5 kV, and the atomic force microscope (AFM) ones are taken by MFP-3D (Asylum Research Company); the surface potential of PVDF nanofibers is measured by AFM in the electrostatic force microscopy mode. The surface potential of the PVDF-ESNF was measured by the electrometer (model 344). The R-TENG is implanted into a rubber mold where the airflow of breath is most concentrated, in which the rubber mold reserved a hole with a diameter of 6 mm. The rubber mold and the filter membrane in the commercial mask are purchased from Protection Specialties Inc (China) and SMJ Inc (China), respectively.

Particulate Matters Generation. The particulate matters generation and the removal efficiency measurement of the testing apparatus for the R-TENG are processed in a 3 m³ acrylic box, and the particulate matters used in this work are generated by burning cigarettes because of the merits such as wide particulates size distribution from 10 nm to 10 μm , low price, and close to the existence of real environment particulates. The SEA-FM is tested in a 4 m² room, in which the density of particulate matter and humidity can be controlled by burning cigarettes and humidifier, respectively.

Removal Efficiency, Pressure, Humidity, and Wind Speed Measurement. Smoke particulate matters are diluted with an air circulator for 10 min as aim to evenly disperse in the inside space of the acrylic box. The airflow concentration of particulate matters is adjusted to a hazardous pollution level, in which the PM2.5 index equals to 500 $\mu\text{g}/\text{m}^3$. A hand-held particulate counter (3016-IAQ, Lighthouse) is employed to detect the particulate matters concentration. A scanning mobility particulate sizer (SMPS3938L75, TSI) and an aerodynamic particulate sizer (3321, TSI) are used to measure the particulates number distribution after 240 min filtration. A portable pressure tester (testo 510) and a humidity tester (testo 174H) are used to monitor the pressure drop and the environmental humidity of the inside box during filtration. The gas speed is tested by a float flowmeter (LZB-10WB). The removal efficiency η , characterizing the filter performance, is determined by the particulate concentration of inlet and outlet, as follows

$$\eta = \left(1 - \frac{C_o}{C_{in}} \right) \times 100\% \quad (1)$$

where C_o is the cumulative mass concentration ($\mu\text{g}/\text{m}^3$) of particulates in the outlet and C_{in} is the cumulative mass concentration ($\mu\text{g}/\text{m}^3$) in the inlet. For example, $\eta_{5.0} = 95.7$ wt % is the ratio between the total mass lost and the total mass on the inlet for all of the particulates with a size less than or equal to 5.0 μm .

ASSOCIATED CONTENT

Supporting Information

The Supporting Information is available free of charge on the ACS Publications website at DOI: 10.1021/acsami.7b18732.

Structure of testing apparatus, finite element simulation of the R-TENG, AFM imagine morphology; SEM images; surface potential of the PVDF-ESNF, and number distribution and removal efficiency of coarse and fine particulates (PDF)

AUTHOR INFORMATION

Corresponding Authors

*E-mail: czhang@binn.cas.cn (C.Z.).

*E-mail: zlwang@gatech.edu (Z.L.W.).

ORCID

Chi Zhang: 0000-0002-7511-805X

Zhong Lin Wang: 0000-0002-5530-0380

Author Contributions

G.L., J.N., and C.H. contributed equally to this work. G.L., J.N., and C.H. designed the experiments. G.L. conducted the electrical performance measurement and also carried out the filtration test with the assistance of J.N. T.J. conducted the FEM with the assistance from Z.Y. G.L. carried out the SEM measurements with the assistance of Y.P. and also performed the AFM characterization with the assistance of L.X. T.G. and C.Z. prepared the manuscript with inputs from all other coauthors and Z.L.W. guided all the experiment.

Notes

The authors declare no competing financial interest.

ACKNOWLEDGMENTS

The authors thank the support of National Key Research and Development Program of China (2016YFA0202704), National Natural Science Foundation of China (no. 51475099), Beijing Nova Program (no. Z171100001117054), the Youth Innovation Promotion Association, CAS (no. 2014033), and the “thousands talents” program for the pioneer researcher and his innovation team, China. National Natural Science Foundation of China (no. 51608039) and Natural Science Foundation of Beijing, China (no. 4154090). The authors also thank Feng Ben Xi, Jun Qing Zhao, and Bo Wu for R-TENGs fabrication and applications demonstration.

REFERENCES

- (1) Künzli, N.; Kaiser, R.; Medina, S.; Studnicka, M.; Chanel, O.; Filliger, P.; Herry, M.; Horak, F.; Puybonnieux-Texier, V.; Quénel, P.; Schneider, J.; Seethaler, R.; Vergnaud, J.-C.; Sommer, H. Public-Health Impact of Outdoor and Traffic-Related Air Pollution: A European Assessment. *Lancet* **2000**, *356*, 795–801.
- (2) Sun, Y.; Zhuang, G.; Wang, Y.; Han, L.; Guo, J.; Dan, M.; Zhang, W.; Wang, Z.; Hao, Z. The Air-Borne Particulate Pollution In Beijing—Concentration, Composition, Distribution and Sources. *Atmos. Environ.* **2004**, *38*, 5991–6004.
- (3) Sadorsky, P. The Effect of Urbanization and Industrialization on Energy Use in Emerging Economies: Implications for Sustainable Development. *Am. J. Econ. Sociol.* **2014**, *73*, 392–409.
- (4) O'Neill, B. C.; Ren, X.; Jiang, L.; Dalton, M. The Effect of Urbanization on Energy Use in India and China in the IPETS Model. *Energy Econ.* **2012**, *34*, S339–S345.
- (5) Thurston, G. D.; Ito, K.; Lall, R. Corrigendum to “A Source Apportionment of U.S. Fine Particulate Matter Air Pollution”. *Atmos. Environ.* **2011**, *47*, 566–569.
- (6) Zhang, Q.; Quan, J.; Tie, X.; Li, X.; Liu, Q.; Gao, Y.; Zhao, D. Effects of Meteorology and Secondary Particle Formation on Visibility During Heavy Haze Events in Beijing, China. *Sci. Total Environ.* **2015**, *502*, 578–584.
- (7) Calderón-Garcidueñas, L.; Solt, A. C.; Henríquez-Roldán, C.; Torres-Jardón, R.; Nuse, B.; Herritt, L.; Villarreal-Calderón, R.; Osnaya, N.; Stone, I.; García, R.; Brooks, D. M.; González-Maciel, A.; Reynoso-Robles, R.; Delgado-Chávez, R.; Reed, W. Long-Term Air Pollution Exposure is Associated with Neuroinflammation, an Altered Innate Immune Response, Disruption of The Blood-Brain Barrier, Ultrafine Particulate Deposition, and Accumulation of Amyloid β -42 and α -Synuclein in Children and Young Adults. *Toxicol. Pathol.* **2008**, *36*, 289–310.
- (8) Ancelet, T.; Davy, P. K.; Trompetter, W. J.; Markwitz, A. Sources of Particulate Matter Pollution in a Small New Zealand city. *Atmos. Pollut. Res.* **2014**, *5*, 572–580.
- (9) Xu, X.; Yavar, Z.; Verdin, M.; Ying, Z.; Mihai, G.; Kampfrath, T.; Wang, A.; Zhong, M.; Lippmann, M.; Chen, L.-C.; Rajagopalan, S.; Sun, Q. Effect of Early Particulate Air Pollution Exposure on Obesity in Mice: Role of P47phox. *Arterioscler., Thromb., Vasc. Biol.* **2010**, *30*, 2518–2527.
- (10) Allen, J. L.; Liu, X.; Pelkowski, S.; Palmer, B.; Conrad, K.; Oberdörster, G.; Weston, D.; Mayer-Pröschel, M.; Cory-Slechta, D. A. Early Postnatal Exposure to Ultrafine Particulate Matter Air Pollution: Persistent Ventriculomegaly, Neurochemical Disruption, and Glial Activation Preferentially in Male Mice. *Environ. Health Perspect.* **2014**, *122*, 939–945.
- (11) Donaldson, K.; Seaton, A. A Short History of the Toxicology of Inhaled Particles. *Part. Fibre Toxicol.* **2012**, *9*, 13.
- (12) Nel, A. Atmosphere: Enhanced: Air Pollution-Related Illness: Effects of Particles. *Science* **2005**, *308*, 804–806.
- (13) Lave, L. B.; Seskin, E. P. Air Pollution and Human Health. *Science* **1970**, *169*, 723–733.
- (14) Zhao, X.; Wang, S.; Yin, X.; Yu, J.; Ding, B. Slip-Effect Functional Air Filter for Efficient Purification of PM2.5. *Sci. Rep.* **2016**, *6*, 35472.
- (15) Feng, Z.; Long, Z.; Yu, T. Filtration Characteristics of Fibrous Filter Following an Electrostatic Precipitator. *J. Electrost.* **2016**, *83*, 52–62.
- (16) Shafeeyan, M. S.; Daud, W. M. A. W.; Houshmand, A.; Shamiri, A. A Review on Surface Modification of Activated Carbon for Carbon Dioxide Adsorption. *J. Anal. Appl. Pyrolysis* **2010**, *89*, 143–151.
- (17) Xi, Y.; Guo, H.; Zi, Y.; Li, X.; Wang, J.; Deng, J.; Li, S.; Hu, C.; Cao, X.; Wang, Z. L. Multifunctional TENG for Blue Energy Scavenging and Self-Powered Wind-Speed Sensor. *Adv. Energy Mater.* **2017**, *7*, 1602397.
- (18) Wang, Z. L. Catch Wave Power in Floating Nets. *Nature* **2017**, *S42*, 159–160.
- (19) Zhang, L. M.; Han, C. B.; Jiang, T.; Zhou, T.; Li, X. H.; Zhang, C.; Wang, Z. L. Multilayer Wavy-Structured Robust Triboelectric Nanogenerator for Harvesting Water Wave Energy. *Nano Energy* **2016**, *22*, 87–94.
- (20) Wang, X.; Niu, S.; Yi, F.; Yin, Y.; Hao, C.; Dai, K.; Zhang, Y.; You, Z.; Wang, Z. L. Harvesting Ambient Vibration Energy over a Wide Frequency Range for Self-Powered Electronics. *ACS Nano* **2017**, *11*, 1728–1735.
- (21) Pu, X.; Li, L.; Song, H.; Du, C.; Zhao, Z.; Jiang, C.; Cao, G.; Hu, W.; Wang, Z. L. A Self-Charging Power Unit by Integration of a Textile Triboelectric Nanogenerator and a Flexible lithium-ion Battery for Wearable Electronics. *Adv. Mater.* **2015**, *27*, 2472–2478.
- (22) Lai, Y.-C.; Deng, J.; Zhang, S. L.; Niu, S.; Guo, H.; Wang, Z. L. Single-Thread-Based Wearable and Highly Stretchable Triboelectric Nanogenerators and Their Applications in Cloth-Based Self-Powered Human-Interactive and Biomedical Sensing. *Adv. Funct. Mater.* **2016**, *27*, 1604462.
- (23) Guo, H.; Yeh, M.-H.; Zi, Y.; Wen, Z.; Chen, J.; Liu, G.; Hu, C.; Wang, Z. L. Ultralight Cut-Paper-Based Self-Charging Power Unit for Self-Powered Portable Electronic and Medical Systems. *ACS Nano* **2017**, *11*, 4475–4482.
- (24) Zhang, C.; Tang, W.; Han, C.; Fan, F.; Wang, Z. L. Theoretical Comparison, Equivalent Transformation, and Conjunction Operations of Electromagnetic Induction Generator and Triboelectric Nanogenerator for Harvesting Mechanical Energy. *Adv. Mater.* **2014**, *26*, 3580–3591.
- (25) Zhang, C.; Zhang, L. M.; Tang, W.; Han, C. B.; Wang, Z. L. Tribotronic Logic Circuits and Basic Operations. *Adv. Mater.* **2015**, *27*, 3533–3540.
- (26) Zhang, C.; Li, J.; Han, C. B.; Zhang, L. M.; Chen, X. Y.; Wang, L. D.; Dong, G. F.; Wang, Z. L. Organic Tribotronic Transistor for Contact-Electrification-Gated Light-Emitting Diode. *Adv. Funct. Mater.* **2015**, *25*, 5625–5632.
- (27) Zhang, C.; Tang, W.; Pang, Y.; Han, C.; Wang, Z. L. Active Micro-Actuators for Optical Modulation based on a Planar Sliding Triboelectric Nanogenerator. *Adv. Mater.* **2015**, *27*, 719–726.
- (28) Zhang, C.; Tang, W.; Zhang, L.; Han, C.; Wang, Z. L. Contact Electrification Field-Effect Transistor. *ACS Nano* **2014**, *8*, 8702–8709.

- (29) Han, C. B.; Jiang, T.; Zhang, C.; Li, X.; Zhang, C.; Cao, X.; Wang, Z. L. Removal of Particulate Matter Emissions from a Vehicle Using a Self-Powered Triboelectric Filter. *ACS Nano* **2015**, *9*, 12552.
- (30) Gu, G. Q.; Han, C. B.; Lu, C. X.; He, C.; Jiang, T.; Gao, Z. L.; Li, C. J.; Wang, Z. L. Triboelectric Nanogenerator Enhanced Nanofiber Air Filters for Efficient Particulate Matter Removal. *ACS Nano* **2017**, *11*, 6211–6217.
- (31) Wang, J.; Li, S.; Yi, F.; Zi, Y.; Lin, J.; Wang, X.; Xu, Y.; Wang, Z. L. Sustainably Powering Wearable Electronics Solely by Biomechanical Energy. *Nat. Commun.* **2016**, *7*, 12744.